

Normalizing Flows are Capable Generative Models

Shuangfei Zhai¹ Ruixiang Zhang¹ Preetum Nakkiran¹ David Berthelot¹ Jiatao Gu¹ Huangjie Zheng¹
Tianrong Chen¹ Miguel Angel Bautista¹ Navdeep Jaitly¹ Josh Susskind¹

Abstract

Normalizing Flows (NFs) are likelihood-based models for continuous inputs. They have demonstrated promising results on both density estimation and generative modeling tasks, but have received relatively little attention in recent years. In this work, we demonstrate that NFs are more powerful than previously believed. We present TARFLOW: a simple and scalable architecture that enables highly performant NF models. TARFLOW can be thought of as a Transformer-based variant of Masked Autoregressive Flows (MAFs): it consists of a stack of autoregressive Transformer blocks on image patches, alternating the autoregression direction between layers. TARFLOW is straightforward to train end-to-end, and capable of directly modeling and generating pixels. We also propose three key techniques to improve sample quality: Gaussian noise augmentation during training, a post training denoising procedure, and an effective guidance method for both class-conditional and unconditional settings. Putting these together, TARFLOW sets new state-of-the-art results on likelihood estimation for images, beating the previous best methods by a large margin, and generates samples with quality and diversity comparable to diffusion models, for the first time with a stand-alone NF model. We make our code available at <https://github.com/apple/ml-tarflow>.

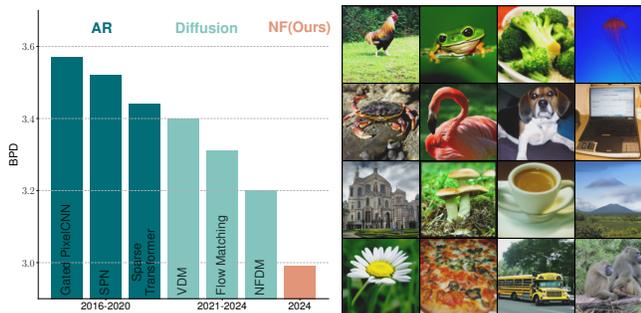


Figure 1. TARFLOW demonstrates substantial progress in the domain of normalizing flow models, achieving state-of-the-art results in both density estimation and sample generation. **Left:** We show the historical progression of likelihood performance on ImageNet 64x64, measured in bits per dimension (BPD), where our model significantly outperforms previous methods (see Table 2 for details). **Right:** Selected samples from our model trained on ImageNet 128x128 demonstrate unprecedented image quality and diversity for a normalizing flow model, establishing a new benchmark for this class of generative models.

distribution (such as Gaussian noise), keeping track of likelihoods via the change of variable formula. Normalizing Flows enjoy many unique and appealing properties, including exact likelihood computation, deterministic objective functions, and efficient computation of both the data generator and its inverse. There has been a large body of work dedicated to studying and improving NFs, and in fact NFs were the method of choice for density estimation for a number of years (Dinh et al., 2017; Kingma & Dhariwal, 2018; Chen et al., 2018; Papamakarios et al., 2017; Ho et al., 2019). However in spite of this rich line of work, Normalizing Flows have seen limited practical adoption—in stark contrast to other generative models such as Diffusion Models (Sohl-Dickstein et al., 2015; Ho et al., 2020) and Large Language Models (Brown et al., 2020). Moreover, the state-of-the-art in Normalizing Flows has not kept pace with the rapid progress of these other generative techniques, leading to less attention from the research community.

It is natural to wonder whether this situation is inherent—i.e., are Normalizing Flows fundamentally limited as a modeling paradigm? Or, have we just not found an appropriate way to train powerful NFs and fully realize their potential?

1. Introduction

Normalizing Flows (NFs) are a well-established likelihood based method for unsupervised learning (Tabak & Vandenberg, 2010; Rezende & Mohamed, 2015; Dinh et al., 2014). The method follows a simple learning objective, which is to transform a data distribution into a simple prior

¹Apple. Correspondence to: Shuangfei Zhai <szhai@apple.com>.

Answering this question may allow us to reopen an alternative path to powerful generative modeling, similar to how DDPM (Ho et al., 2020) enlightened the field of diffusion modeling and brought about its current renaissance.

In this work, we show that NFs are more powerful than previously believed, and in fact can compete with state-of-the-art generative models on images. Specifically, we introduce TARFLOW (short for Transformer AutoRegressive Flow): a powerful NF architecture that allows one to easily scale up the model’s capacity; as well as a set of techniques that drastically improve the model’s generation capability.

On the architecture side, TARFLOW is conceptually similar to Masked Autoregressive Flows (MAFs) (Papamakarios et al., 2017), where we compose a deep transformation by iteratively stacking multiple blocks of autoregressive transformations with alternating directions. The key difference is that we deploy a powerful masked Transformer (Vaswani et al., 2017) based implementation that operates in a block autoregression fashion (that is, predicting a block of dimensions at a time), instead of simple masked MLPs used in MAFs that factorizes the input on a per dimension basis.

In the context of image modeling, we implement each autoregressive flow transformation with a causal Vision Transformer (ViT) (Dosovitskiy et al., 2021) on top of a sequence of image patches, given a particular order of autoregression (e.g., top left to bottom right, or the reverse). This admits a powerful non-linear transformation among all image patches, while maintaining a parallel computational graph during training. Compared to other NF design choices (Dinh et al., 2017; Grathwohl et al., 2019; Kingma & Dhariwal, 2018; Ho et al., 2019) which often have several types of interleaving modules, our model features a modular design and enjoys greater simplicity, both conceptually and practically. This in return allows for much improved scalability and training stability, which is another critical aspect for high performance models. With this new architecture, we can immediately train much stronger NF models than previously reported, resulting in state-of-the-art results on image likelihood estimation.

On the generation side, we introduce three important techniques. First, we show that for perceptual quality, it is critical to add a moderate amount of Gaussian noise to the inputs, in contrast to a small amount of uniform noise commonly used in the literature. Second, we identify a post-training score based denoising technique that allows one to remove the noise portion of the generated samples. Third, we show for the first time that guidance (Ho & Salimans, 2022) is compatible with NF models, and we propose guidance recipes for both the class conditional and unconditional models. Putting these techniques together, we are able to achieve state-of-the-art sample quality for NF models on standard image modeling tasks.

We highlight our main results in Figure 1, and summarize our contributions as follows.

- We introduce TARFLOW, a simple and powerful Transformer based Normalizing Flow architecture.
- We achieve state-of-the-art results on likelihood estimation on images, achieving a sub-3 BPD on ImageNet 64x64 for the first time.
- We show that Gaussian noise augmentation during training plays a critical role in producing high quality samples.
- We present a post-training score-based denoising technique that allows one to remove the noise in the generated samples.
- We show that guidance is compatible with both class conditional and unconditional models, which drastically improves sampling quality.

Table 1. Notation.

Notation	Meaning
$p_{\text{data}}(x)$	training distribution
$p_{\text{model}}(y)$	model distribution
$f(x)$	the forward flow function
$f^t(z^t)$	the forward function for the t -th flow block
μ^t, α^t	learnable causal functions in the t -th flow block
$p_\epsilon(\epsilon)$	the noise distribution
$q(y)$	the noisy data distribution
$\tilde{p}(\tilde{x})$	the discrete model distribution

2. Method

2.1. Normalizing Flows

Given continuous inputs $x \sim p_{\text{data}}$, $x \in \mathbb{R}^D$, a Normalizing Flow learns a density p_{model} via the change of variable formula $p_{\text{model}}(x) = p_0(f(x))|\det(\frac{df(x)}{dx})|$, where $f: \mathbb{R}^D \mapsto \mathbb{R}^D$ is an invertible transformation for which we can also compute the determinant of the Jacobian $\det(\frac{df(x)}{dx})$; p_0 is a prior distribution. The maximum likelihood estimation (MLE) objective can then be written as

$$\min_f -\log p_0(f(x)) - \log(|\det(\frac{df(x)}{dx})|). \quad (1)$$

In this paper, we let p_0 be a standard Gaussian distribution $\mathcal{N}(0, I_D)$, so Equation 1 can be explicitly written as

$$\min_f 0.5\|f(x)\|_2^2 - \log(|\det(\frac{df(x)}{dx})|), \quad (2)$$

where we have omitted constant terms. Equation 2 bears an intuitive interpretation: the first term encourages the model

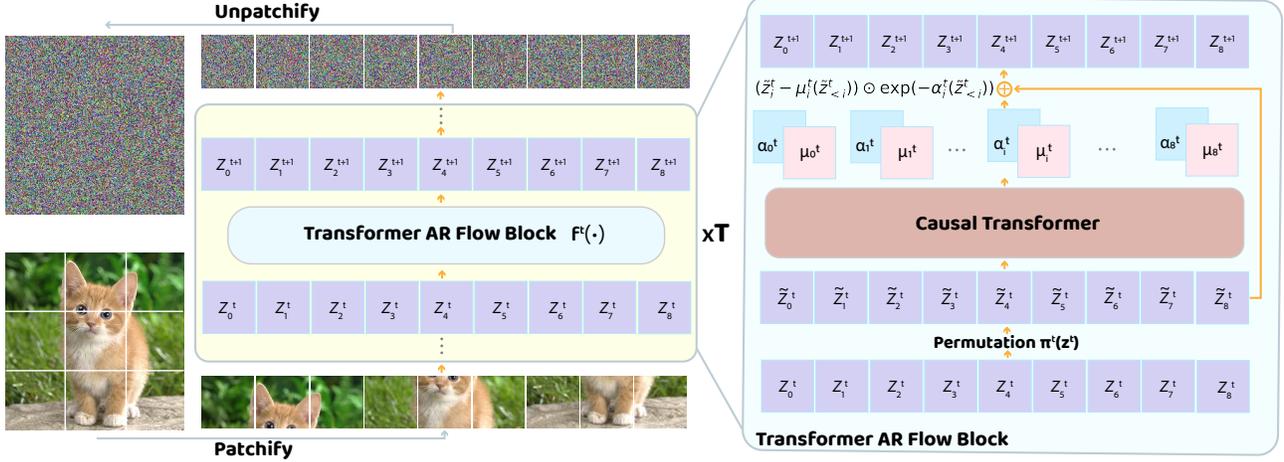


Figure 2. **Left**, TARFLOW consists of T flow blocks trained end to end; **Right**, a zoom-in view of each flow block, which contains a sequence permutation operation, a standard causal Transformer, and an affine transformation to the permuted inputs.

to map data samples x to latent variables $z = f(x)$ of small norm, while the second term discourages the model from “collapsing” — i.e., the model should map proximate inputs to separated latents which allows it to fully occupy the latent space. Once the model is trained, one automatically obtains a generative model via $z \sim p_0(z)$, $x = f^{-1}(z)$.

2.2. Block Autoregressive Flows

One appealing method for constructing a deep normalizing flow is by stacking multiple layers of autoregressive flows. This was first proposed in IAF (Kingma et al., 2016) in the context of variational inference, and later extended by MAF (Papamakarios et al., 2017) as standalone density models.

In this paper, we consider a generalized formulation of MAF — block autoregressive flows. Without loss of generality, we assume an input presented in the form of a sequence $x \in \mathbb{R}^{N \times D}$, where N is the sequence length and D is the dimension of each block of input. Let $T \in \mathbb{N}$ be the number of flow layers in the stack of flows. Subscripts denote indexing along the sequence dimension, e.g. $x_i \in \mathbb{R}^D$, and superscripts denotes flow-layer indices (see Figure 2). We then specify a flow transformation $z^T = f(x) := (f^{T-1} \circ f^{T-2} \dots \circ f^0)(x)$ as follows. First, we choose $\{\pi^t\}$ as any fixed set of permutation functions along the sequence dimension. The t -th flow, f^t , is parameterized by two learnable functions $\mu^t, \alpha^t : \mathbb{R}^{N \times D} \rightarrow \mathbb{R}^{N \times D}$, which are both causal along the sequence dimension.

We initialize with $z^0 := x$. Then, the t -th flow transforms $z^t \in \mathbb{R}^{N \times D}$ into $z^{t+1} \in \mathbb{R}^{N \times D}$ by transforming a block of

inputs $\{z_i^t\}_{i \in [N]}$ as:

$$\begin{aligned} \tilde{z}^t &\leftarrow \pi^t(z^t), \\ z_i^{t+1} &\leftarrow \begin{cases} \tilde{z}_i^t & i = 0 \\ (\tilde{z}_i^t - \mu_i^t(\tilde{z}_{<i}^t)) \odot \exp(-\alpha_i^t(\tilde{z}_{<i}^t)) & i > 0 \end{cases} \end{aligned} \quad (3)$$

Note that since μ^t is causal, the i -token of its output $\mu_i^t(\tilde{z}^t)$ only depends on $\tilde{z}_{<i}^t$, as written explicitly above. Iterating the above for $t = 0, 1, \dots, (T-1)$ yields the output $z^T =: f(x)$. The inverse function $x = f^{-1}(z^T)$ is given by iterating the following flow to obtain z^t from z^{t+1} :

$$\begin{aligned} \tilde{z}_i^t &= \begin{cases} z_i^{t+1}, & i = 0 \\ z_i^{t+1} \odot \exp(\alpha_i^t(\tilde{z}_{<i}^t)) + \mu_i^t(\tilde{z}_{<i}^t) & i > 0 \end{cases} \quad (4) \\ z^t &= (\pi^t)^{-1}(\tilde{z}^t). \end{aligned}$$

This yields $x := z^0$ as the final iterate. As for the choice of permutations π^t , in this work we set all π^t as the reverse function $\pi^t(z)_i = z_{N-1-i}$, except for π^0 which is set as identity. Ultimately, the entire flow transformation consists of T flows $\{f^t\}$, and in each flow the input is first permuted then causally transformed with learnable element-wise subtractive and divisive terms $\mu_i^t(\cdot)$, $\exp(\alpha_i^t(\cdot))$.

It is worth noting that Equation 3 degenerates to MAF when $D = 1$. Intuitively, D plays a role of balancing the difficulty of modeling each position in the sequence and the length of the entire sequence. This allows for extra modeling flexibility compared to the naive setting in MAF, which will become clearer in the later discussions.

In each flow transformation f^t , there are two operations. The first permutation operation π^t is volume preserving, therefore its log determinant of the Jacobian is zero. The second autoregressive step has a Jacobian matrix of lower

triangular shape, which means its determinant needs to only account for the diagonal entries. The log determinant of the Jacobian then readily evaluates to

$$\log(|\det(\frac{df^t(z^t)}{dz^t})|) = - \sum_{i=1}^{N-1} \sum_{j=0}^{D-1} \alpha_i^t (z_{<i}^t)_j. \quad (5)$$

Putting them together, the training loss of our model can be written as

$$\min_f 0.5 \|z^T\|_2^2 + \sum_{t=0}^{T-1} \sum_{i=1}^{N-1} \sum_{j=0}^{D-1} \alpha_i^t (z_{<i}^t)_j, \quad (6)$$

which simply consists of a square term and a sum of linear terms.

2.3. Transformer Autoregressive Flows

Architecture design is arguably the most challenging aspect of NF models. We suspect that a large part of the reason that NFs have not been as performant as other families of models is the lack of an architecture that allows for stable and scalable training.

To this end, we resort to a Transformer-based architecture, TARFLOW, with a design philosophy that features simplicity and modularity. In particular, we realize the fact that Equation 3 favors a parallel implementation with attention masks. This follows the same spirit as the original MAFs, but we replace the MLP based implementation with a much more powerful Transformer backbone which has a proven track record of success across both discrete and continuous domains. This seemingly simple change allows one to fully unlock the potentials of autoregressive flows, to a degree that has never been previously shown or expected.

We now consider the concrete case of modeling images, with the discussions generalizable to other domains. Given an image of shape $C \times H \times W$, where C, H, W are the channel size, height and width of the image, respectively, we first convert it to a sequence of patches with a patch size of S . This gives us a sequence representation of $x \in \mathbb{R}^{N \times D}$, $N = \frac{HW}{S^2}$, $D = CS^2$. Similarly, the input of each flow transform z^t will have the same size as x . We can then readily apply a standard Vision Transformer with causal attention masks to implement the transformation of a single autoregressive pass f^t . Importantly, the Transformer can have arbitrary depth and width, completely independent of the input’s dimension.

When stacking multiple autoregressive transformations, the entire model can be viewed as a variant of a Residual Network. More specifically, the network consists of two types of residual connections: the first over the hidden layers inside the causal Transformer, the second over the latents z_i^t . This ensures another important factor of the architecture

design: training stability — i.e., training our model should be as easy as training a standard Transformer.

Combining the architecture and the loss (Equation 6) together, we have a complete recipe for a simple, scalable, and trainable NF model. See Figure 2 for an illustration of the architecture.

2.4. Noise Augmented Training

It is considered a common practice to introduce additive noise to the inputs during the training of NF models (Dinh et al., 2017; Ho et al., 2019). The usage of noise has mostly been motivated from the likelihood perspective, where adding uniform noise whose width is the same as the pixel quantization bin size to images allows one to “dequantize” the discrete pixel distribution to a continuous one. Formally speaking, instead of directly modeling the training data distribution p_{data} , we model a noise augmented distribution $q(y) = \int_{\epsilon} p_{\text{data}}(y - \epsilon) p_{\epsilon}(\epsilon) d\epsilon$. With a finite training set \mathcal{X} , this can be explicitly rewritten as $q(y) = \frac{1}{|\mathcal{X}|} \sum_{x \in \mathcal{X}} p_{\epsilon}(y - x)$. When evaluating likelihood, we follow the literature (Dinh et al., 2017) and let $p_{\epsilon}(\cdot) = \mathcal{U}(\cdot; 0, \text{bin})$, where bin is the quantization bin size (e.g., $\frac{1}{128}$ for 8-bit pixels normalized to the range of $[-1, 1]$). We can then compute likelihood w.r.t. the discrete inputs \tilde{x} with $\tilde{p}(\tilde{x}) = \int_{\epsilon \in [0, \text{bin}]^D} p_{\text{model}}(\tilde{x} + \epsilon) d\epsilon$.

For better perceptual quality during sampling, however, we show that it is critical to set $p_{\epsilon}(\cdot)$ as a Gaussian distribution $\mathcal{N}(\cdot; 0, \sigma^2 \mathbf{I})$ whose magnitude σ is small but larger than that of the pixel quantization bin size. To put it into context, with image pixels in $[-1, 1]$, an optimal σ of $p_{\epsilon}(\cdot)$ for sample quality is around 0.05, whereas the standard deviation of the dequantization uniform noise is merely 0.002, an order of magnitude smaller.

Why is this the case? There are two factors which could be important. First, training a NF model with good generalization is inherently a challenging task. Without adding noise, the inverse model $f^{-1}(z)$ is effectively trained on discretized inputs z , of the same size as the training set. During the inference, however, f^{-1} is expected to generalize on a much denser input distribution (e.g., Gaussian), which poses an out-of-distribution problem that hinders the sampling quality. Adding noise therefore serves a simple purpose of enriching the support of the training distribution, hence the support of the inverse model f^{-1} . Second, using a Gaussian noise instead of uniform is also critical, as the former effectively stretches the support of the training distribution to the ambient input space, with the mode of the density placed at the original data points. Although this makes it less straightforward to convert the learned density $q(y)$ to a discrete data probability, but we will later see that it greatly enhances the sampling quality.



Figure 3. Images of various resolutions generated by TARFLOW models. From left to right, top to bottom: 256x256 images on AFHQ, 128x128 and 64x64 images on ImageNet.

2.5. Score Based Denoising

Training with noise augmentation introduces an additional challenge: models trained on the noisy distribution $q(y)$ naturally generate outputs that mimic noisy training examples, rather than clean ones. This results in samples that are less visually appealing. As a remedy, we propose a straightforward training-free technique that effectively denoises the generated samples, by drawing inspiration from score-based generative models.

The idea is as follows. Consider the joint distribution (x, y) where $x \sim p_{\text{data}}$ and $y = x + \varepsilon$ for $\varepsilon \sim \mathcal{N}(0, \sigma^2 \mathbf{I})$. By definition, y is marginally distributed as the noisy data distribution q . By Tweedie’s formula, we have

$$\mathbb{E}[x | y] = y + \sigma^2 \nabla_y \log q(y). \quad (7)$$

Therefore, given a noisy sample y we can denoise it to a clean sample $\hat{x} := \mathbb{E}[x | y]$ if we know gradients of the log-likelihood $\log q(y)$. Under the condition when σ is small, we have $\mathbb{E}[x | y] \approx x$. Now further assuming that the model $p_{\text{model}}(\cdot)$ is well trained, we can use the same formula to denoise a sample from the model, using p_{model} in place of q . The complete sampling procedure can be written as:

$$z \sim p_0, y := f^{-1}(z), x := y + \sigma^2 \nabla_y \log p_{\text{model}}(y). \quad (8)$$

2.6. Guidance

An important property of state-of-the-art generative models is their ability to be controlled during inference. Normalizing flows have conventionally relied on low temperature sampling (Kingma & Dhariwal, 2018), but it’s only applicable to the volume preserving variants and also introduces severe smoothing artifacts.

On the other hand, guidance in diffusion models (Dhariwal & Nichol, 2021; Ho & Salimans, 2022) have achieved great success in this regard, which allows one to trade-off diversity for improved mode seeking ability. Surprisingly, we found that our models can also be guided, offering very similar flexibility to the case in diffusion models.

Conditional Guidance In the conditional generation setting, guidance can be obtained in almost the exact same way as classifier free guidance (CFG) (Ho & Salimans, 2022) in diffusion models. We first override the notation by letting $\mu_i^t(\cdot; c)$, $\alpha_i^t(\cdot; c)$ be the class conditional predictions, and $\mu_i^t(\cdot; \emptyset)$, $\alpha_i^t(\cdot; \emptyset)$ be the unconditional counterparts. In practice, the unconditional predictions can be obtained by randomly dropping out the class label during training, similar to (Ho & Salimans, 2022). For each flow block t , we modify the reverse function in Equation 4 to

$$\tilde{z}_i^t = z_i^{t+1} \odot \exp(\tilde{\alpha}_i^t(\tilde{z}_{<i}^t; c, w)) + \tilde{\mu}_i^t(\tilde{z}_{<i}^t; c, w). \quad (9)$$

Here we generate \tilde{z}_i^t with the guided predictions $\tilde{\mu}_i^t(\cdot; c, w)$, $\tilde{\alpha}_i^t(\cdot; c, w)$ under guidance weight w , which are defined as

$$\begin{aligned} \tilde{\mu}_i^t(\tilde{z}_{<i}^t; c, w) &= (1 + w)\mu_i^t(\tilde{z}_{<i}^t; c) - w\mu_i^t(\tilde{z}_{<i}^t; \emptyset), \\ \tilde{\alpha}_i^t(\tilde{z}_{<i}^t; c, w) &= (1 + w)\alpha_i^t(\tilde{z}_{<i}^t; c) - w\alpha_i^t(\tilde{z}_{<i}^t; \emptyset). \end{aligned} \quad (10)$$

Intuitively, under positive guidance $w > 0$, Equation 10 modifies the updates of sampling to guide conditional variables \tilde{z}_i^t away from predictions from an unconditional model, therefore converging more towards the class model of c .

Unconditional Guidance In addition, we also introduce a novel method for guiding unconditional models. The

basic idea is to construct predictions of inferior quality, analogous to the role of unconditional ones. In order to do so, we override the notation yet again and introduce $\mu_i^t(\cdot; \tau), \alpha_i^t(\cdot; \tau)$. Here we have let the predictions μ_i^t, α_i^t take an additional parameter τ , which corresponds to a manually injected temperature term to all the attention layers in the Transformer for f^t . Namely, for each attention layer in f^t , we divide the attention logits by τ , before normalizing it with the Softmax function. A τ larger or smaller than 1 makes the attention overly smooth or sharp, either way reducing the Transformer’s ability to correctly predict the next variable’s transformations.

We can then similarly write out the unconditional guided predictions as

$$\begin{aligned} \tilde{\mu}_i^t(\tilde{z}_{<i}^t; \tau, w) &= (1 + w)\mu_i^t(\tilde{z}_{<i}^t; 1) - w\mu_i^t(\tilde{z}_{<i}^t; \tau), \\ \tilde{\alpha}_i^t(\tilde{z}_{<i}^t; \tau, w) &= (1 + w)\alpha_i^t(\tilde{z}_{<i}^t; 1) - w\alpha_i^t(\tilde{z}_{<i}^t; \tau), \end{aligned} \quad (11)$$

where increasing either w or $|\tau - 1|$ corresponds to stronger guidance.

Lastly, for both the conditional and unconditional cases, it is possible to assign a different guidance weight w_i^t depending on the flow and position index t, i . We have preliminarily explored a linearly increased w_i as a function of i , as in $w_i = \frac{i}{T-1}w$, and we have found this to achieve better sampling results w.r.t. FID than uniform guidance weights. We leave the thorough exploration of the optimal guidance schedule as future work.

3. Experiments

We perform our experiments on unconditional ImageNet 64x64 (van den Oord et al., 2016b), as well as class conditional ImageNet 64x64, ImageNet 128x128 (Deng et al., 2009) and AFHQ 256x256 (Choi et al., 2020).

Our models are implemented as stacks of standard causal Vision Transformers (Dosovitskiy et al., 2021). In each AR flow block, the inputs are first linearly projected to the model channel size, then added with learned position embeddings. For class conditional models, we add an immediate class embedding on top of it. We use attention head dimensions of 64 and an MLP latent size $4 \times$ that of the model channel size. The output layer of each flow block consists of two heads per position, corresponding to μ_i^t, α_i^t , respectively, and they are initialized as zeros. All parameters are trained end-to-end with the AdamW optimizer with momentum (0.9, 0.95). We use a cosine learning rate schedule, where the learning rate is warmed up from 10^{-6} to 10^{-4} for one epoch, then decayed to 10^{-6} . We use a small weight decay of 10^{-4} to stabilize training.

We adopt a simple data preprocessing protocol, where we center crop images and linearly rescale the pixels to $[-1, 1]$. For each task, we search for architecture configurations

Table 2. Bits per dim evaluation on unconditional ImageNet 64x64 test set. We denote the TARFLOW configuration in the format [P-Ch-T-K- p_ϵ].

Model	Type	BPD ↓
Very Deep VAE (Child, 2021)	VAE	3.52
Glow (Kingma & Dhariwal, 2018)	Flow	3.81
Flow++ (Ho et al., 2019)	Flow	3.69
PixelCNN (van den Oord et al., 2016a)	AR	3.83
SPN (Menick & Kalchbrenner, 2019)	AR	3.52
Sparse Transformer (Child et al., 2019)	AR	3.44
Routing Transformer (Roy et al., 2021)	AR	3.43
Improved DDPM (Nichol & Dhariwal, 2021)	Diff/FM	3.54
VDM (Kingma et al., 2021)	Diff/FM	3.40
Flow Matching (Lipman et al., 2023a)	Diff/FM	3.31
NFDM (Bartosh et al., 2024)	Diff/FM	3.20
TARFLOW [2-768-8-8- $\mathcal{U}(0, \frac{1}{128})$] (Ours)	NF	2.99

consisting of the patch size (P), model channel size (Ch), number of autoregressive flow blocks (T) and the number of attention layers in each flow (K). For generation tasks, we also search for the best input noise σ that yields the best sampling quality. We denote a TARFLOW configuration as P-Ch-T-K- p_ϵ .

Our model significantly advances the state-of-the-art in likelihood modeling, achieving substantial improvements over previous methods. At the same time, TARFLOW demonstrates unprecedented sample generation quality for the class of normalizing flow models, reaching levels comparable to diffusion models and GANs for the first time. Detailed experimental configurations are provided in the Appendix.

3.1. Likelihood

Likelihood estimation provides a direct assessment of a normalizing flow architecture’s modeling capacity, as it aligns precisely with the model’s training objective. For evaluating likelihood on image data, unconditional ImageNet 64x64 has acted as the de facto benchmark dataset. Its relatively large scale and inherent diversity pose significant challenges for model fitting, making it an ideal testbed where improvements typically stem from enhanced model capacity rather than regularization techniques.

During both training and evaluation, we apply uniform noise $\mathcal{U}(0, \frac{1}{128})$ to the data, which corresponds to the “dequantization” noise (Dinh et al., 2017). We do not use any additional data augmentation techniques during training. As shown in Table 2 and visualized in Figure 1, our approach establishes new state-of-the-art result in test set likelihood, by a significant margin over all previous models.

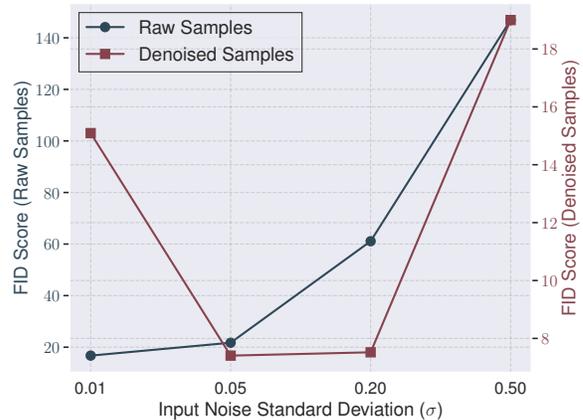
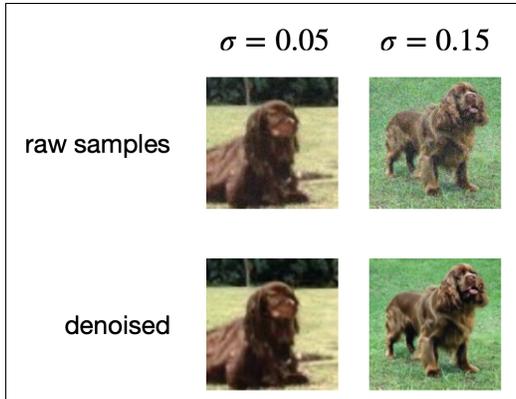


Figure 4. **Left:** The effect of input noise σ and denoising, all samples are generated with guidance weight $w = 2$ on ImageNet 128x128 from the same initial noise, better viewed when zoomed in. **Right:** Sample FID vs input noise σ on ImageNet 64x64, with and without denoising. Before denoising, it first appears that small σ has the best FID, due to the smaller amount of noise present in the raw samples. However, after denoising with Equation 8, slightly larger σ favors better FID and demonstrates more consistent shapes. Note that the *scale* of the right y-axis differs from that of the left.

Table 3. Fréchet Inception Distance (FID) evaluation on Conditional ImageNet 64x64. We denote the TARFLOW configuration in the format [P-Ch-T-K- p_ϵ].

Model	Type	FID ↓
EDM (Karras et al., 2022)	Diff/FM	1.55
iDDPM (Nichol & Dhariwal, 2021)	Diff/FM	2.92
ADM(dropout) (Dhariwal & Nichol, 2021)	Diff/FM	2.09
IC-GAN (Casanova et al., 2021)	GAN	6.70
BigGAN (Brock et al., 2019)	GAN	4.06
CD(LPIPS)(Song et al., 2023)	CM	4.70
iCT-deep(Song & Dhariwal, 2023)	CM	3.25
TARFLOW [4-1024-8-8- $\mathcal{N}(0, 0.05^2)$] (Ours)	NF	3.99
TARFLOW [2-768-8-8- $\mathcal{N}(0, 0.05^2)$] (Ours)	NF	2.90

Table 4. Fréchet Inception Distance (FID) evaluation on Unconditional ImageNet 64x64. We denote the TARFLOW configuration in the format [P-Ch-T-K- p_ϵ].

Model	Type	FID ↓
MFM (Pooladian et al., 2023)	Diff/FM	11.82
FM (Lipman et al., 2023b)	Diff/FM	13.93
AGM (Chen et al., 2024)	Diff/FM	10.07
IC-GAN (Casanova et al., 2021)	GAN	10.40
Self-sup GAN (Noroozi, 2020)	GAN	19.20
TARFLOW [2-768-8-8- $\mathcal{N}(0, 0.05^2)$] (Ours)	NF	18.42

3.2. Generation

Next, we evaluate TARFLOW’s sampling ability in class conditional (ImageNet 64x64, ImageNet 128x128, AFHQ 256x256) as well as unconditional (ImageNet 64x64) settings. Our experimental protocol is largely the same as

Table 5. Fréchet Inception Distance (FID) evaluation on Conditional ImageNet 128x128. We denote the TARFLOW configuration in the format [P-Ch-T-K- p_ϵ].

Model	Type	FID ↓
ADM-G (Dhariwal & Nichol, 2021)	Diff/FM	2.97
CDM (Ho et al., 2022)	Diff/FM	3.52
Simple Diff (Hoogeboom et al., 2023)	Diff/FM	1.94
RIN (Jabri et al., 2023)	Diff/FM	2.75
BigGAN (Brock et al., 2019)	GAN	8.70
BigGAN-deep (Brock et al., 2019)	GAN	5.70
TARFLOW [4-1024-8-8- $\mathcal{N}(0, 0.05^2)$] (Ours)	NF	5.29
TARFLOW [4-1024-8-8- $\mathcal{N}(0, 0.15^2)$] (Ours)	NF	5.03

previously mentioned, except that we adopt random horizontal image flips. For the class conditional models, we randomly drop the class label with a probability of 0.1.

We first show qualitative results in Figure 3, which are obtained with the sampling procedure in Equation 8. We see that TARFLOW generates diverse and high fidelity images in all settings. Also, TARFLOW seems to demonstrate great robustness w.r.t. the data size and resolution. For instance, it works well on both a large diverse dataset (ImageNet, $\sim 1.3M$ examples, 1K classes) and a small but high resolution one (AFHQ, 15K examples in 3 classes and 256x256). Visually, these samples are comparable to those generated by Diffusion Models, which marks a large improvement from the previous best NF models. We include more qualitative results in the Appendix.

We then perform quantitative evaluations in terms of FID, on the ImageNet models. For each setting, we randomly generate 50K samples, and compare it with the statistics



Figure 5. Guidance weight w vs FID for both the conditional and unconditional models (with $\tau = 1.5$) on ImageNet 64x64. Note the y axis’s scale difference between the two settings.

from the entire training set. We search for the best guidance weights (and attention temperature in the unconditional case). The results are summarized in Table 3, 4, 5. In all settings, we see that TARFLOW produces competitive FID numbers, often times better than strong GAN baselines, and approaching results from recent Diffusion Models. It is also interesting to note that we found no publicly reported NF based FID numbers on the ImageNet level datasets, most likely due to the lack of presentable results from the NF community.

3.3. Ablation on Noise Augmentation and Denoising

We then study the role of input noise p_ϵ . We first experimented with the ‘dequantization’ uniform noise and found that sampling experiences constant numerical issues and was not able to produce sensible outputs. We hypothesize the reason being that a narrow uniform noise makes the flow transformation ill-conditioned, as it forces a model to map a low entropy distribution to an ambient Gaussian distribution.

Next, we experiment with different Gaussian noise levels σ during training on class conditional ImageNet 64x64. We use an architecture configuration of 4-1024-8-8, and vary σ in $\{0.01, 0.05, 0.2, 0.5\}$. For fast experimentation, we train all models for only 100 epochs with a batch size of 512. We evaluate these models with a guidance $w = 2$ and plot the 50K sample FIDs before and after the score based denoising. For visual comparison, we also train two models ImageNet 128x128 models, with the architecture 4-1024-8-8 and noise $\sigma \in [0.05, 0.15]$, respectively. We show the FID curves together with the visual examples in Figure 4. There are two important observations. First, naively increasing the noise level on the surface appears to hurt the raw samples’ quality. However, this is no longer

the case after applying the denoising step in Equation 8. Denoising successfully cleans up the noisy raw samples, and as a result the best visual quality occurs at a moderate (but still relatively small) amount of noise. This verifies the necessity of our proposed sampling procedure, whereas the combination of noise augmented training and the score based denoising step work organically together to produce the best generative capability.

3.4. Ablation on Guidance

We then turn our eyes to guidance. Similar to CFG in Diffusion Models, guidance for TARFLOW is a post training technique that allows us to vary the model’s sample quality during inference. We perform qualitative and quantitative evaluations on both the class conditional and unconditional versions of ImageNet 64x64. The results are shown in Figure 5 and 6. In terms of FID, the guidance weight w plays an effective role for both models. Visually, it is also clear that guidance allows the model to converge to more recognizable modes, presenting more aesthetic samples. Interestingly, this is also somewhat true for the unconditional models, whereas both the guidance weight w and attention temperature τ contribute to the degree of guidance. We show more guidance comparisons in the Appendix.

3.5. Ablation on Model Scaling

Another important aspect of our work is the model’s scaling properties. We first show a typical training loss curve together with an online monitoring of the model’s sample quality in terms of FID (we use 4096 samples for efficiency). This is shown in Figure 7(a). We see that the loss curve is smooth and monotonic, and it has a strong positive correlation with the FID curve.

We proceed to discuss another design question: the model’s size, especially model’s depth. Depth plays a vital role in our model, as we need to have a sufficient number of flow blocks, as well as number of layers within each block. This deep transformation then poses questions on architecture design as well as its trainability.

We answer this question by performing two sets of ablations on conditional ImageNet 64x64. In the first set of experiments, we train a set of models who share the same number of combined layers $T \times K$; and in the second, we increase a base model’s depth by increasing either T or K . The results are shown in Figure 7(b). First of all, we observe again the strong positive correlation between the loss and FID curves, across different architectures. This points to a nice property of NF models where improving the likelihood (i.e., the loss) directly leads to improved generative modeling capabilities. Second, there is a U-shape distribution w.r.t. the $T \times K$ configuration, and it appears that the best trade-off occurs when $T = K$. The case of $T = 1$ is also interesting, as it



Figure 6. **Left:** Varying guidance weight with the class conditional model on ImageNet 128x128, here we show 4 samples from the ImageNet class 849 (“teapot”); **Right:** Varying guidance weight and attention temperature for the unconditional ImageNet 64x64 model.

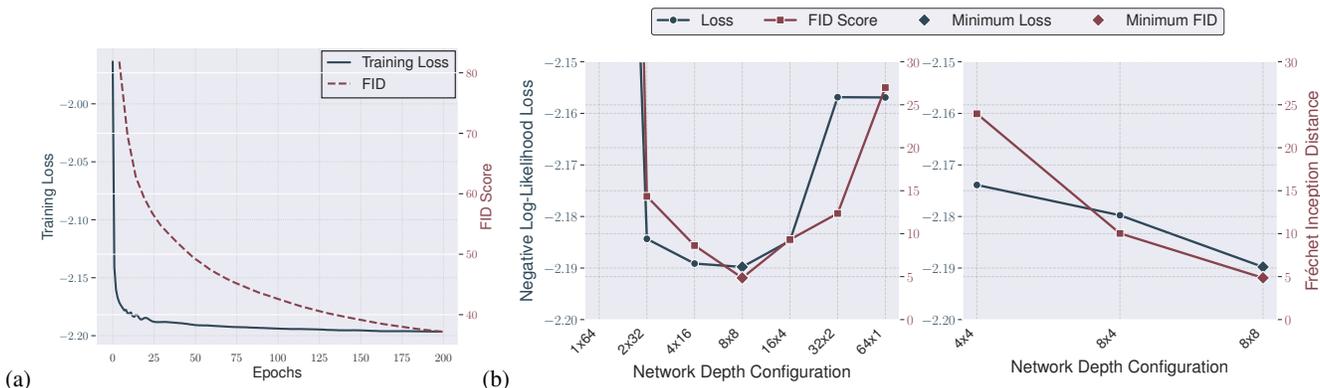


Figure 7. (a) A typical training run on ImageNet 64x64. Our loss smoothly decreases during training, and is positively correlated with FID. (b) Depth configuration (in the form of $T \times K$) vs training loss. Overall, we see a strong positive correlation between the training loss and FID. **Left,** the optimal training loss happens when the capacity is evenly allocated to number of blocks and number of layers per block. Interestingly, the special case of 1 block degenerates to an incapable model, which has both high loss and FID equivalent to random guess. **Right,** increasing both the number of blocks and number of layers per block improves the model’s loss and sampling quality.

corresponds to a special case of a single direction autoregressive model on image patches. It is obvious that this model fails to fit the data, both in terms of loss and FID. This is in contrast to the $T = 2$ configuration which has a much more reasonable performance. Lastly, increasing either T or K is effective in improving the model’s capacity. Putting these observations together, we see that TARFLOW demonstrates promising scaling behaviors, which makes it a particularly appealing candidate for exploiting the wide abundance of power of modern compute infrastructures.

3.6. Visualizing Sample Trajectory

Lastly, thanks to the residual style composition of TARFLOW, we can also visualize the generation process by reshaping each $\{z^t\}$ to the pixel space. We visualize two sampling sequences with the ImageNet 128x128 model in Figure 8. Interestingly, the sample trajectories highly resemble those from a Diffusion model, in the sense that the initial noise is gradually transformed into visible inputs – though they are trained with completely different objectives.

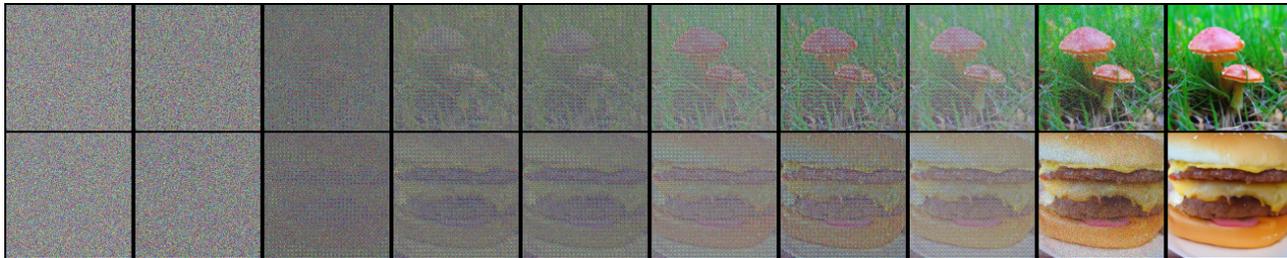


Figure 8. From left to right, the sampling trajectory from the model on ImageNet 128x128 with 8 flow blocks. The visualization includes the final denoising step.

4. Related Work

Coupling-based Normalizing Flows Many research endeavors focus on developing expressive invertible transformations with tractable Jacobian computations for constructing normalizing flows. NICE (Dinh et al., 2014) introduced additive coupling layers to construct the transformations and simplified the computation of the Jacobian determinant. RealNVP (Dinh et al., 2017) extended this approach by incorporating scaling and shifting operations to enhance the model’s expressiveness. Glow (Kingma & Dhariwal, 2018) advanced these models by introducing invertible 1×1 convolutions, achieving improved results in image generation tasks. Flow++ (Ho et al., 2019) further introduced attention mechanisms to enhance the model’s expressiveness. iResNet (Behrmann et al., 2019) demonstrated the invertibility of standard ResNet architectures (He et al., 2016) by incorporating a normalization step. Moreover, normalizing flows have played an important role in improving the performance of Variational Autoencoders (VAEs) (Kingma & Welling, 2014) by providing flexible posterior distributions (Su & Wu, 2018; Zhang et al., 2020), and in diffusion models (Song et al., 2021b) by introducing adaptable nonlinear forward and backward diffusion and drift terms (Kim et al., 2022). What’s shared in common among these designs is that they need carefully wired and restrictive architectures, which poses great a challenge in scaling the model’s capacity.

Continuous Normalizing Flows Neural Ordinary Differential Equations (Chen et al., 2018) reformulate the standard ResNet architecture as a deterministic ordinary differential equation in the continuous-time limit. This formulation can be naturally extended to normalizing flows, resulting in Continuous Normalizing Flows. In this framework, the invertibility of the network is inherently satisfied, and the computation of the Jacobian determinant within the normalizing flow is reduced to calculating the trace of the Jacobian. By leveraging Pontryagin’s Maximum Principle (Pontryagin, 1988), gradient backpropagation through such networks can be efficiently performed using the adjoint method, which requires only $\mathcal{O}(1)$ memory complexity. FFIORD (Grathwohl et al., 2019) further simplifies the expensive Jacobian

computation by employing Hutchinson’s trace estimator (Hutchinson, 1989). However, these models often suffer from numerical instability during training and sampling, which has been extensively analyzed in (Zhuang et al., 2021; Liu et al., 2021). The expressive capability can be further improved by augmenting auxiliary variables (Dupont et al., 2019; Chalvidal et al., 2021). In comparison, TARFLOW enables an unconstrained architecture design paradigm by fully taking advantage of the power of causal Transformers, which we believe is a key component for realizing the true potential of the NF principle.

Autoregressive Normalizing Flows There have also been significant efforts to integrate normalizing flows with autoregressive models. IAF (Kingma et al., 2016) introduced dimension-wise affine transformations conditioned on preceding dimensions for variational inference, and MAF (Papamakarios et al., 2017) leveraged the MADE (Germain et al., 2015) architecture to construct invertible mappings through autoregressive transformations. Neural autoregressive flow (Huang et al., 2018) replaces the affine transformation in MAF by parameterizing a monotonic neural network for each dimension to enhance the transformation’s expressiveness, at the cost of losing analytical invertibility. T-NAF (Patacchiola et al., 2024) extends NAF by introducing a single autoregressive Transformer. Block Neural Autoregressive Flow (Cao et al., 2019) takes a different approach by fitting an end-to-end autoregressive monotonic neural network, rather than NAF’s dimension-wise sequence parameterization, but also sacrifices analytical invertibility. TARFLOW differs from these as we show that it is sufficient to stack multiple iterations of block autoregressive flows with standard Transformer model in alternating directions, without the need for other types of flow operations.

Probability Flow in Diffusion Diffusion models (Sohl-Dickstein et al., 2015; Ho et al., 2020; Song et al., 2021b) generate data by simulating Stochastic Differential Equations. Song et al. (2021b) provided a deterministic Ordinary Differential Equation counterpart to this generative approach, also known as the scoreflow (Song et al., 2021a).

The scoreflow can be understood as a special case of continuous normalizing flows by interpreting the learned score term and base drift as a new parameterized drift term. However, Lu et al. (2022) demonstrated that the training objective in diffusion models, which relies on first-order score approximation, is not sufficient to maximize the likelihood of the scoreflow. TARFLOW differs from these instances as it is directly trained with the MLE objective, without the need for excessively large Gaussian noise during training.

Autoregressive Models for Image Generation Many efforts (van den Oord et al., 2016b;a; Esser et al., 2021; Razavi et al., 2019) have been made to apply autoregressive sequential methods to image generation. PixelRNN(van den Oord et al., 2016b) is a pioneering work in this field. This approach views an image as a sequence of data, modeling the distribution of each subsequent pixel conditioned on all previously generated pixels through an RNN architecture(Sherstinsky, 2020). This methodology is readily adaptable to masked convolutional structures(van den Oord et al., 2016a), where the prediction of the next pixel is based on its neighboring pixels, bypassing the use of a traditional convolutional kernel. The transformer model has been successfully applied to image generation tasks. Chen et al. (2020) introduced ImageGPT, an autoregressive model that predicts pixels sequentially in raster order. More recently, Yu et al. (2022) introduced Parti, a scalable encoder-decoder transformer for text-to-image generation, which conceptualizes the task as a sequence-to-sequence problem. VAR(Tian et al., 2024) begins with low-resolution images in the latent space, effectively predicting the next level of resolution and yielding impressive outcomes. Studies like (Yu et al., 2022; Gu et al., 2024; Sun et al., 2024) further demonstrate the scalability and effectiveness of autoregressive models in producing high-dimensional images. Recent work MAR (Li et al., 2024) introduced diffusion models for autoregressive latent token prediction as an alternative to vector quantization approaches for image generation. GIVT (Tschannen et al., 2025) employed transformer decoders to model latent tokens generated by a VAE encoder, while incorporating a Gaussian Mixture Model (GMM) in place of categorical prediction for likelihood modeling. Concurrently to our work, JetFormer (Tschannen et al., 2024) further extended the approach by substituting the VAE with a coupling-based normalizing flow model, and used an autoregressive Transformer with GIVT’s GMM prediction head to model sequences of latent tokens. While TARFLOW employs a causal Transformer architecture similar to these approaches, it operates differently by processing continuous data directly with a single model, thus avoiding the complexity of input discretization, or the need for separate image tokenization and autoregressive modeling stages.

Diffusion models, other generative models Diffusion models (Ho et al., 2020; Song et al., 2021b) are emerging generative models that achieve appealing results. Stable Diffusion (Podell et al., 2024) and OpenSora (Zheng et al., 2024) push the boundaries of diffusion models’ capabilities, demonstrating their ability to generate extremely high-dimensional data. Besides, Variational Autoencoders (VAEs) (Kingma & Welling, 2014) and Generative Adversarial Networks (GANs) (Goodfellow et al., 2014) are also popular generative models. By avoiding the posterior collapse issue, VQ-VAE (van den Oord et al., 2017) demonstrates impressive generative performance and subsequently serves as an essential component in the later latent diffusion model (Podell et al., 2024). In the realm of GANs, Karras et al. (2019); Kang et al. (2023); Brock et al. (2019) showcase the remarkable capability of GANs to generate high-resolution images with comparatively cheap inference costs, though the training stability of GANs remains challenging (Wiatrak et al., 2019). TARFLOW represents an orthogonal learning paradigm to these methods, with its unique benefits and challenges.

5. Conclusion

We presented TARFLOW, a Transformer-based architecture together with a set of techniques that allows us to train high-performance normalizing flow models. Our model achieves state-of-the-art results on likelihood estimation, improving upon the previous best results by a large margin. We also show competitive sampling performance, qualitatively and quantitatively, and demonstrate for the first time that normalizing flows alone are a capable generative modeling technique. We hope that our work can inspire future interest in further pushing the envelope of simple and scalable generative modeling principles.

6. Acknowledgements

We thank Yizhe Zhang, Alaa El-Nouby, Arwen Bradley, Yuyang Wang, and Laurent Dinh for helpful discussions. We also thank Samy Bengio for leadership support that made this work possible.

References

- Bartosh, G., Vetrov, D., and Naesseth, C. A. Neural flow diffusion models: Learnable forward process for improved diffusion modelling. *ArXiv preprint, abs/2404.12940*, 2024. URL <https://arxiv.org/abs/2404.12940>.
- Behrmann, J., Grathwohl, W., Chen, R. T. Q., Duvenaud, D., and Jacobsen, J. Invertible residual networks. In Chaudhuri, K. and Salakhutdinov, R. (eds.), *Pro-*

- ceedings of the 36th International Conference on Machine Learning, ICML 2019, 9-15 June 2019, Long Beach, California, USA*, volume 97 of *Proceedings of Machine Learning Research*, pp. 573–582. PMLR, 2019. URL <http://proceedings.mlr.press/v97/behrmann19a.html>.
- Brock, A., Donahue, J., and Simonyan, K. Large scale GAN training for high fidelity natural image synthesis. In *7th International Conference on Learning Representations, ICLR 2019, New Orleans, LA, USA, May 6-9, 2019*. OpenReview.net, 2019. URL <https://openreview.net/forum?id=Blxsqj09Fm>.
- Brown, T. B., Mann, B., Ryder, N., Subbiah, M., Kaplan, J., Dhariwal, P., Neelakantan, A., Shyam, P., Sastry, G., Askell, A., Agarwal, S., Herbert-Voss, A., Krueger, G., Henighan, T., Child, R., Ramesh, A., Ziegler, D. M., Wu, J., Winter, C., Hesse, C., Chen, M., Sigler, E., Litwin, M., Gray, S., Chess, B., Clark, J., Berner, C., McCandlish, S., Radford, A., Sutskever, I., and Amodei, D. Language models are few-shot learners. In Larochelle, H., Ranzato, M., Hadsell, R., Balcan, M., and Lin, H. (eds.), *Advances in Neural Information Processing Systems 33: Annual Conference on Neural Information Processing Systems 2020, NeurIPS 2020, December 6-12, 2020, virtual*, 2020. URL <https://proceedings.neurips.cc/paper/2020/hash/1457c0d6bfc4967418bfb8ac142f64a-Abstract.html>.
- Cao, N. D., Aziz, W., and Titov, I. Block neural autoregressive flow. In Globerson, A. and Silva, R. (eds.), *Proceedings of the Thirty-Fifth Conference on Uncertainty in Artificial Intelligence, UAI 2019, Tel Aviv, Israel, July 22-25, 2019*, volume 115 of *Proceedings of Machine Learning Research*, pp. 1263–1273. AUAI Press, 2019. URL <http://proceedings.mlr.press/v115/de-cao20a.html>.
- Casanova, A., Careil, M., Verbeek, J., Drozdal, M., and Romero-Soriano, A. Instance-conditioned GAN. In Ranzato, M., Beygelzimer, A., Dauphin, Y. N., Liang, P., and Vaughan, J. W. (eds.), *Advances in Neural Information Processing Systems 34: Annual Conference on Neural Information Processing Systems 2021, NeurIPS 2021, December 6-14, 2021, virtual*, pp. 27517–27529, 2021. URL <https://proceedings.neurips.cc/paper/2021/hash/e7ac288b0f2d41445904d071ba37aaff-Abstract.html>.
- Chalvidal, M., Ricci, M., VanRullen, R., and Serre, T. Go with the flow: Adaptive control for neural odes. In *9th International Conference on Learning Representations, ICLR 2021, Virtual Event, Austria, May 3-7, 2021*. OpenReview.net, 2021. URL <https://openreview.net/forum?id=giit4HdDNa>.
- Chen, M., Radford, A., Child, R., Wu, J., Jun, H., Luan, D., and Sutskever, I. Generative pretraining from pixels. In *Proceedings of the 37th International Conference on Machine Learning, ICML 2020, 13-18 July 2020, Virtual Event*, volume 119 of *Proceedings of Machine Learning Research*, pp. 1691–1703. PMLR, 2020. URL <http://proceedings.mlr.press/v119/chen20s.html>.
- Chen, T., Gu, J., Dinh, L., Theodorou, E., Susskind, J. M., and Zhai, S. Generative modeling with phase stochastic bridge. In *The Twelfth International Conference on Learning Representations, 2024*.
- Chen, T. Q., Rubanova, Y., Bettencourt, J., and Duvenaud, D. Neural ordinary differential equations. In Bengio, S., Wallach, H. M., Larochelle, H., Grauman, K., Cesa-Bianchi, N., and Garnett, R. (eds.), *Advances in Neural Information Processing Systems 31: Annual Conference on Neural Information Processing Systems 2018, NeurIPS 2018, December 3-8, 2018, Montréal, Canada*, pp. 6572–6583, 2018. URL <https://proceedings.neurips.cc/paper/2018/hash/69386f6bb1dfed68692a24c8686939b9-Abstract.html>.
- Child, R. Very deep vaes generalize autoregressive models and can outperform them on images. In *9th International Conference on Learning Representations, ICLR 2021, Virtual Event, Austria, May 3-7, 2021*. OpenReview.net, 2021. URL <https://openreview.net/forum?id=RLRXCV6DbEJ>.
- Child, R., Gray, S., Radford, A., and Sutskever, I. Generating long sequences with sparse transformers. *ArXiv preprint*, abs/1904.10509, 2019. URL <https://arxiv.org/abs/1904.10509>.
- Choi, Y., Uh, Y., Yoo, J., and Ha, J. Stargan v2: Diverse image synthesis for multiple domains. In *2020 IEEE/CVF Conference on Computer Vision and Pattern Recognition, CVPR 2020, Seattle, WA, USA, June 13-19, 2020*, pp. 8185–8194. IEEE, 2020. doi: 10.1109/CVPR42600.2020.00821. URL <https://doi.org/10.1109/CVPR42600.2020.00821>.
- Deng, J., Dong, W., Socher, R., Li, L., Li, K., and Li, F. Imagenet: A large-scale hierarchical image database. In *2009 IEEE Computer Society Conference on Computer Vision and Pattern Recognition (CVPR 2009), 20-25 June 2009, Miami, Florida, USA*, pp. 248–255. IEEE Computer Society, 2009. doi: 10.1109/CVPR.2009.5206848. URL <https://doi.org/10.1109/CVPR.2009.5206848>.

- Dhariwal, P. and Nichol, A. Q. Diffusion models beat gans on image synthesis. In Ranzato, M., Beygelzimer, A., Dauphin, Y. N., Liang, P., and Vaughan, J. W. (eds.), *Advances in Neural Information Processing Systems 34: Annual Conference on Neural Information Processing Systems 2021, NeurIPS 2021, December 6-14, 2021, virtual*, pp. 8780–8794, 2021. URL <https://proceedings.neurips.cc/paper/2021/hash/49ad23d1ec9fa4bd8d77d02681df5cfa-Abstract.html>.
- Dinh, L., Krueger, D., and Bengio, Y. Nice: Non-linear independent components estimation. *International Conference on Learning Representations workshop Track*, 2014.
- Dinh, L., Sohl-Dickstein, J., and Bengio, S. Density estimation using real NVP. In *5th International Conference on Learning Representations, ICLR 2017, Toulon, France, April 24-26, 2017, Conference Track Proceedings*. OpenReview.net, 2017. URL <https://openreview.net/forum?id=HkpbN91x>.
- Dosovitskiy, A., Beyer, L., Kolesnikov, A., Weissenborn, D., Zhai, X., Unterthiner, T., Dehghani, M., Minderer, M., Heigold, G., Gelly, S., Uszkoreit, J., and Houlsby, N. An image is worth 16x16 words: Transformers for image recognition at scale. In *9th International Conference on Learning Representations, ICLR 2021, Virtual Event, Austria, May 3-7, 2021*. OpenReview.net, 2021. URL <https://openreview.net/forum?id=YicbFdNTTy>.
- Dupont, E., Doucet, A., and Teh, Y. W. Augmented neural odes. In Wallach, H. M., Larochelle, H., Beygelzimer, A., d’Alché-Buc, F., Fox, E. B., and Garnett, R. (eds.), *Advances in Neural Information Processing Systems 32: Annual Conference on Neural Information Processing Systems 2019, NeurIPS 2019, December 8-14, 2019, Vancouver, BC, Canada*, pp. 3134–3144, 2019. URL <https://proceedings.neurips.cc/paper/2019/hash/21be9a4bd4f81549a9d1d241981cec3c-Abstract.html>.
- Esser, P., Rombach, R., and Ommer, B. Taming transformers for high-resolution image synthesis. In *IEEE Conference on Computer Vision and Pattern Recognition, CVPR 2021, virtual, June 19-25, 2021*, pp. 12873–12883. Computer Vision Foundation / IEEE, 2021. doi: 10.1109/CVPR46437.2021.01268. URL https://openaccess.thecvf.com/content/CVPR2021/html/Esser_Taming_Transformers_for_High-Resolution_Image_Synthesis_CVPR_2021_paper.html.
- Germain, M., Gregor, K., Murray, I., and Larochelle, H. MADE: masked autoencoder for distribution estimation. In Bach, F. R. and Blei, D. M. (eds.), *Proceedings of the 32nd International Conference on Machine Learning, ICML 2015, Lille, France, 6-11 July 2015*, volume 37 of *JMLR Workshop and Conference Proceedings*, pp. 881–889. JMLR.org, 2015. URL <http://proceedings.mlr.press/v37/germain15.html>.
- Goodfellow, I. J., Pouget-Abadie, J., Mirza, M., Xu, B., Warde-Farley, D., Ozair, S., Courville, A. C., and Bengio, Y. Generative adversarial nets. In Ghahramani, Z., Welling, M., Cortes, C., Lawrence, N. D., and Weinberger, K. Q. (eds.), *Advances in Neural Information Processing Systems 27: Annual Conference on Neural Information Processing Systems 2014, December 8-13 2014, Montreal, Quebec, Canada*, pp. 2672–2680, 2014. URL <https://proceedings.neurips.cc/paper/2014/hash/5ca3e9b122f61f8f06494c97b1afccf3-Abstract.html>.
- Grathwohl, W., Chen, R. T. Q., Bettencourt, J., Sutskever, I., and Duvenaud, D. FFDJORD: free-form continuous dynamics for scalable reversible generative models. In *7th International Conference on Learning Representations, ICLR 2019, New Orleans, LA, USA, May 6-9, 2019*. OpenReview.net, 2019. URL <https://openreview.net/forum?id=rJxgknCck7>.
- Gu, J., Wang, Y., Zhang, Y., Zhang, Q., Zhang, D., Jaitly, N., Susskind, J., and Zhai, S. Dart: Denoising autoregressive transformer for scalable text-to-image generation. *ArXiv preprint*, abs/2410.08159, 2024. URL <https://arxiv.org/abs/2410.08159>.
- He, K., Zhang, X., Ren, S., and Sun, J. Deep residual learning for image recognition. In *2016 IEEE Conference on Computer Vision and Pattern Recognition, CVPR 2016, Las Vegas, NV, USA, June 27-30, 2016*, pp. 770–778. IEEE Computer Society, 2016. doi: 10.1109/CVPR.2016.90. URL <https://doi.org/10.1109/CVPR.2016.90>.
- Ho, J. and Salimans, T. Classifier-free diffusion guidance. *ArXiv preprint*, abs/2207.12598, 2022. URL <https://arxiv.org/abs/2207.12598>.
- Ho, J., Chen, X., Srinivas, A., Duan, Y., and Abbeel, P. Flow++: Improving flow-based generative models with variational dequantization and architecture design. In Chaudhuri, K. and Salakhutdinov, R. (eds.), *Proceedings of the 36th International Conference on Machine Learning, ICML 2019, 9-15 June 2019, Long Beach, California, USA*, volume 97 of *Proceedings of Machine Learning Research*, pp. 2722–2730. PMLR, 2019. URL <http://proceedings.mlr.press/v97/ho19a.html>.

- Ho, J., Jain, A., and Abbeel, P. Denoising diffusion probabilistic models. In Larochelle, H., Ranzato, M., Hadsell, R., Balcan, M., and Lin, H. (eds.), *Advances in Neural Information Processing Systems 33: Annual Conference on Neural Information Processing Systems 2020, NeurIPS 2020, December 6-12, 2020, virtual*, 2020. URL <https://proceedings.neurips.cc/paper/2020/hash/4c5bcfec8584af0d967f1ab10179ca4b-Abstract.html>.
- Ho, J., Saharia, C., Chan, W., Fleet, D. J., Norouzi, M., and Salimans, T. Cascaded diffusion models for high fidelity image generation. *J. Mach. Learn. Res.*, 23:47:1–47:33, 2022. URL <http://jmlr.org/papers/v23/21-0635.html>.
- Hoogeboom, E., Heek, J., and Salimans, T. simple diffusion: End-to-end diffusion for high resolution images. In Krause, A., Brunskill, E., Cho, K., Engelhardt, B., Sabato, S., and Scarlett, J. (eds.), *International Conference on Machine Learning, ICML 2023, 23-29 July 2023, Honolulu, Hawaii, USA*, volume 202 of *Proceedings of Machine Learning Research*, pp. 13213–13232. PMLR, 2023. URL <https://proceedings.mlr.press/v202/hoogeboom23a.html>.
- Huang, C., Krueger, D., Lacoste, A., and Courville, A. C. Neural autoregressive flows. In Dy, J. G. and Krause, A. (eds.), *Proceedings of the 35th International Conference on Machine Learning, ICML 2018, Stockholmsmässan, Stockholm, Sweden, July 10-15, 2018*, volume 80 of *Proceedings of Machine Learning Research*, pp. 2083–2092. PMLR, 2018. URL <http://proceedings.mlr.press/v80/huang18d.html>.
- Hutchinson, M. F. A stochastic estimator of the trace of the influence matrix for laplacian smoothing splines. *Communications in Statistics-Simulation and Computation*, 18(3):1059–1076, 1989.
- Jabri, A., Fleet, D. J., and Chen, T. Scalable adaptive computation for iterative generation. In Krause, A., Brunskill, E., Cho, K., Engelhardt, B., Sabato, S., and Scarlett, J. (eds.), *International Conference on Machine Learning, ICML 2023, 23-29 July 2023, Honolulu, Hawaii, USA*, volume 202 of *Proceedings of Machine Learning Research*, pp. 14569–14589. PMLR, 2023. URL <https://proceedings.mlr.press/v202/jabri23a.html>.
- Kang, M., Zhu, J., Zhang, R., Park, J., Shechtman, E., Paris, S., and Park, T. Scaling up gans for text-to-image synthesis. In *IEEE/CVF Conference on Computer Vision and Pattern Recognition, CVPR 2023, Vancouver, BC, Canada, June 17-24, 2023*, pp. 10124–10134. IEEE, 2023. doi: 10.1109/CVPR52729.2023.00976. URL <https://doi.org/10.1109/CVPR52729.2023.00976>.
- Karras, T., Laine, S., and Aila, T. A style-based generator architecture for generative adversarial networks. In *IEEE Conference on Computer Vision and Pattern Recognition, CVPR 2019, Long Beach, CA, USA, June 16-20, 2019*, pp. 4401–4410. Computer Vision Foundation / IEEE, 2019. doi: 10.1109/CVPR.2019.00453. URL http://openaccess.thecvf.com/content_CVPR_2019/html/Karras_A_Style-Based_Generator_Architecture_for_Generative_Adversarial_Networks_CVPR_2019_paper.html.
- Karras, T., Aittala, M., Aila, T., and Laine, S. Elucidating the design space of diffusion-based generative models. In Koyejo, S., Mohamed, S., Agarwal, A., Belgrave, D., Cho, K., and Oh, A. (eds.), *Advances in Neural Information Processing Systems 35: Annual Conference on Neural Information Processing Systems 2022, NeurIPS 2022, New Orleans, LA, USA, November 28 - December 9, 2022*, 2022.
- Kim, D., Na, B., Kwon, S. J., Lee, D., Kang, W., and Moon, I. Maximum likelihood training of implicit nonlinear diffusion model. In Koyejo, S., Mohamed, S., Agarwal, A., Belgrave, D., Cho, K., and Oh, A. (eds.), *Advances in Neural Information Processing Systems 35: Annual Conference on Neural Information Processing Systems 2022, NeurIPS 2022, New Orleans, LA, USA, November 28 - December 9, 2022*, 2022.
- Kingma, D., Salimans, T., Poole, B., and Ho, J. Variational diffusion models. *Advances in neural information processing systems*, 34:21696–21707, 2021.
- Kingma, D. P. and Dhariwal, P. Glow: Generative flow with invertible 1x1 convolutions. In Bengio, S., Wallach, H. M., Larochelle, H., Grauman, K., Cesa-Bianchi, N., and Garnett, R. (eds.), *Advances in Neural Information Processing Systems 31: Annual Conference on Neural Information Processing Systems 2018, NeurIPS 2018, December 3-8, 2018, Montréal, Canada*, pp. 10236–10245, 2018. URL <https://proceedings.neurips.cc/paper/2018/hash/d139db6a236200b21cc7f752979132d0-Abstract.html>.
- Kingma, D. P. and Welling, M. Auto-encoding variational bayes. In Bengio, Y. and LeCun, Y. (eds.), *2nd International Conference on Learning Representations, ICLR 2014, Banff, AB, Canada, April 14-16, 2014, Conference Track Proceedings*, 2014. URL <http://arxiv.org/abs/1312.6114>.

- Kingma, D. P., Salimans, T., Jozefowicz, R., Chen, X., Sutskever, I., and Welling, M. Improved variational inference with inverse autoregressive flow. *Advances in neural information processing systems*, 29, 2016.
- Li, T., Tian, Y., Li, H., Deng, M., and He, K. Autoregressive image generation without vector quantization. *ArXiv preprint*, abs/2406.11838, 2024. URL <https://arxiv.org/abs/2406.11838>.
- Lipman, Y., Chen, R. T. Q., Ben-Hamu, H., Nickel, M., and Le, M. Flow matching for generative modeling. In *The Eleventh International Conference on Learning Representations, ICLR 2023, Kigali, Rwanda, May 1-5, 2023*. OpenReview.net, 2023a. URL <https://openreview.net/pdf?id=PqvMRDCJT9t>.
- Lipman, Y., Chen, R. T. Q., Ben-Hamu, H., Nickel, M., and Le, M. Flow matching for generative modeling. In *The Eleventh International Conference on Learning Representations, ICLR 2023, Kigali, Rwanda, May 1-5, 2023*. OpenReview.net, 2023b. URL <https://openreview.net/pdf?id=PqvMRDCJT9t>.
- Liu, G., Chen, T., and Theodorou, E. A. Second-order neural ODE optimizer. In Ranzato, M., Beygelzimer, A., Dauphin, Y. N., Liang, P., and Vaughan, J. W. (eds.), *Advances in Neural Information Processing Systems 34: Annual Conference on Neural Information Processing Systems 2021, NeurIPS 2021, December 6-14, 2021, virtual*, pp. 25267–25279, 2021. URL <https://proceedings.neurips.cc/paper/2021/hash/d4c2e4a3297fe25a71d030b67eb83bfc-Abstract.html>.
- Lu, C., Zheng, K., Bao, F., Chen, J., Li, C., and Zhu, J. Maximum likelihood training for score-based diffusion odes by high order denoising score matching. In Chaudhuri, K., Jegelka, S., Song, L., Szepesvári, C., Niu, G., and Sabato, S. (eds.), *International Conference on Machine Learning, ICML 2022, 17-23 July 2022, Baltimore, Maryland, USA*, volume 162 of *Proceedings of Machine Learning Research*, pp. 14429–14460. PMLR, 2022. URL <https://proceedings.mlr.press/v162/lu22f.html>.
- Menick, J. and Kalchbrenner, N. Generating high fidelity images with subscale pixel networks and multidimensional upscaling. In *7th International Conference on Learning Representations, ICLR 2019, New Orleans, LA, USA, May 6-9, 2019*. OpenReview.net, 2019. URL <https://openreview.net/forum?id=HylzTiC5Km>.
- Nichol, A. Q. and Dhariwal, P. Improved denoising diffusion probabilistic models. In Meila, M. and Zhang, T. (eds.), *Proceedings of the 38th International Conference on Machine Learning, ICML 2021, 18-24 July 2021, Virtual Event*, volume 139 of *Proceedings of Machine Learning Research*, pp. 8162–8171. PMLR, 2021. URL <http://proceedings.mlr.press/v139/nichol21a.html>.
- Noroozi, M. Self-labeled conditional gans. *ArXiv preprint*, abs/2012.02162, 2020. URL <https://arxiv.org/abs/2012.02162>.
- Papamakarios, G., Murray, I., and Pavlakou, T. Masked autoregressive flow for density estimation. In Guyon, I., von Luxburg, U., Bengio, S., Wallach, H. M., Fergus, R., Vishwanathan, S. V. N., and Garnett, R. (eds.), *Advances in Neural Information Processing Systems 30: Annual Conference on Neural Information Processing Systems 2017, December 4-9, 2017, Long Beach, CA, USA*, pp. 2338–2347, 2017. URL <https://proceedings.neurips.cc/paper/2017/hash/6c1da886822c67822bcf3679d04369fa-Abstract.html>.
- Patacchiola, M., Shysheya, A., Hofmann, K., and Turner, R. E. Transformer neural autoregressive flows. *ArXiv preprint*, abs/2401.01855, 2024. URL <https://arxiv.org/abs/2401.01855>.
- Podell, D., English, Z., Lacey, K., Blattmann, A., Dockhorn, T., Müller, J., Penna, J., and Rombach, R. Sdxl: Improving latent diffusion models for high-resolution image synthesis. In *The Twelfth International Conference on Learning Representations*, 2024.
- Pontryagin, L. S. *Mathematical theory of optimal processes*. Routledge, 2018.
- Pooladian, A., Ben-Hamu, H., Domingo-Enrich, C., Amos, B., Lipman, Y., and Chen, R. T. Q. Multisample flow matching: Straightening flows with minibatch couplings. In Krause, A., Brunskill, E., Cho, K., Engelhardt, B., Sabato, S., and Scarlett, J. (eds.), *International Conference on Machine Learning, ICML 2023, 23-29 July 2023, Honolulu, Hawaii, USA*, volume 202 of *Proceedings of Machine Learning Research*, pp. 28100–28127. PMLR, 2023. URL <https://proceedings.mlr.press/v202/pooladian23a.html>.
- Razavi, A., van den Oord, A., and Vinyals, O. Generating diverse high-fidelity images with VQ-VAE-2. In Wallach, H. M., Larochelle, H., Beygelzimer, A., d’Alché-Buc, F., Fox, E. B., and Garnett, R. (eds.), *Advances in Neural Information Processing Systems 32: Annual Conference on Neural Information Processing Systems 2019, NeurIPS 2019, December 8-14, 2019, Vancouver, BC, Canada*, pp. 14837–14847, 2019. URL <https://proceedings.neurips.cc/paper/2019/hash/>

- 5f8e2fa1718d1bbcadf1cd9c7a54fb8c-Abstract.html.
- Rezende, D. J. and Mohamed, S. Variational inference with normalizing flows. In Bach, F. R. and Blei, D. M. (eds.), *Proceedings of the 32nd International Conference on Machine Learning, ICML 2015, Lille, France, 6-11 July 2015*, volume 37 of *JMLR Workshop and Conference Proceedings*, pp. 1530–1538. JMLR.org, 2015. URL <http://proceedings.mlr.press/v37/rezende15.html>.
- Roy, A., Saffar, M., Vaswani, A., and Grangier, D. Efficient content-based sparse attention with routing transformers. *Transactions of the Association for Computational Linguistics*, 9:53–68, 2021. doi: 10.1162/tacl-a.00353. URL <https://aclanthology.org/2021.tacl-1.4>.
- Sherstinsky, A. Fundamentals of recurrent neural network (rnn) and long short-term memory (lstm) network. *Physica D: Nonlinear Phenomena*, 404:132306, 2020.
- Sohl-Dickstein, J., Weiss, E. A., Maheswaranathan, N., and Ganguli, S. Deep unsupervised learning using nonequilibrium thermodynamics. In Bach, F. R. and Blei, D. M. (eds.), *Proceedings of the 32nd International Conference on Machine Learning, ICML 2015, Lille, France, 6-11 July 2015*, volume 37 of *JMLR Workshop and Conference Proceedings*, pp. 2256–2265. JMLR.org, 2015. URL <http://proceedings.mlr.press/v37/sohl-dickstein15.html>.
- Song, Y. and Dhariwal, P. Improved techniques for training consistency models. In *The Twelfth International Conference on Learning Representations*, 2023.
- Song, Y., Durkan, C., Murray, I., and Ermon, S. Maximum likelihood training of score-based diffusion models. In Ranzato, M., Beygelzimer, A., Dauphin, Y. N., Liang, P., and Vaughan, J. W. (eds.), *Advances in Neural Information Processing Systems 34: Annual Conference on Neural Information Processing Systems 2021, NeurIPS 2021, December 6-14, 2021, virtual*, pp. 1415–1428, 2021a. URL <https://proceedings.neurips.cc/paper/2021/hash/0a9fd9bb17feb6ccb7ec405cfb85222c4-Abstract.html>.
- Song, Y., Sohl-Dickstein, J., Kingma, D. P., Kumar, A., Ermon, S., and Poole, B. Score-based generative modeling through stochastic differential equations. In *9th International Conference on Learning Representations, ICLR 2021, Virtual Event, Austria, May 3-7, 2021*. OpenReview.net, 2021b. URL <https://openreview.net/forum?id=PxtIG12RRHS>.
- Song, Y., Dhariwal, P., Chen, M., and Sutskever, I. Consistency models. In Krause, A., Brunskill, E., Cho, K., Engelhardt, B., Sabato, S., and Scarlett, J. (eds.), *International Conference on Machine Learning, ICML 2023, 23-29 July 2023, Honolulu, Hawaii, USA*, volume 202 of *Proceedings of Machine Learning Research*, pp. 32211–32252. PMLR, 2023. URL <https://proceedings.mlr.press/v202/song23a.html>.
- Su, J. and Wu, G. f-vaes: Improve vaes with conditional flows. *ArXiv preprint*, abs/1809.05861, 2018. URL <https://arxiv.org/abs/1809.05861>.
- Sun, P., Jiang, Y., Chen, S., Zhang, S., Peng, B., Luo, P., and Yuan, Z. Autoregressive model beats diffusion: Llama for scalable image generation. *CoRR*, abs/2406.06525, 2024. doi: 10.48550/ARXIV.2406.06525. URL <https://doi.org/10.48550/arXiv.2406.06525>.
- Tabak, E. G. and Vanden-Eijnden, E. Density estimation by dual ascent of the log-likelihood. *Communications in Mathematical Sciences*, 8(1):217–233, 2010.
- Tian, K., Jiang, Y., Yuan, Z., Peng, B., and Wang, L. Visual autoregressive modeling: Scalable image generation via next-scale prediction. *ArXiv preprint*, abs/2404.02905, 2024. URL <https://arxiv.org/abs/2404.02905>.
- Tschannen, M., Pinto, A. S., and Kolesnikov, A. Jet-former: An autoregressive generative model of raw images and text. *ArXiv preprint*, abs/2411.19722, 2024. URL <https://arxiv.org/abs/2411.19722>.
- Tschannen, M., Eastwood, C., and Mentzer, F. Givt: Generative infinite-vocabulary transformers. In *European Conference on Computer Vision*, pp. 292–309. Springer, 2025.
- van den Oord, A., Kalchbrenner, N., Espeholt, L., Kavukcuoglu, K., Vinyals, O., and Graves, A. Conditional image generation with pixelcnn decoders. In Lee, D. D., Sugiyama, M., von Luxburg, U., Guyon, I., and Garnett, R. (eds.), *Advances in Neural Information Processing Systems 29: Annual Conference on Neural Information Processing Systems 2016, December 5-10, 2016, Barcelona, Spain*, pp. 4790–4798, 2016a. URL <https://proceedings.neurips.cc/paper/2016/hash/b1301141feffabac455e1f90a7de2054-Abstract.html>.
- van den Oord, A., Kalchbrenner, N., and Kavukcuoglu, K. Pixel recurrent neural networks. In Balcan, M. and Weinberger, K. Q. (eds.), *Proceedings of the 33rd International Conference on Machine Learning, ICML*

2016, New York City, NY, USA, June 19-24, 2016, volume 48 of *JMLR Workshop and Conference Proceedings*, pp. 1747–1756. JMLR.org, 2016b. URL <http://proceedings.mlr.press/v48/oord16.html>.

van den Oord, A., Vinyals, O., and Kavukcuoglu, K. Neural discrete representation learning. In Guyon, I., von Luxburg, U., Bengio, S., Wallach, H. M., Fergus, R., Vishwanathan, S. V. N., and Garnett, R. (eds.), *Advances in Neural Information Processing Systems 30: Annual Conference on Neural Information Processing Systems 2017, December 4-9, 2017, Long Beach, CA, USA*, pp. 6306–6315, 2017. URL <https://proceedings.neurips.cc/paper/2017/hash/7a98af17e63a0ac09ce2e96d03992fbc-Abstract.html>.

Vaswani, A., Shazeer, N., Parmar, N., Uszkoreit, J., Jones, L., Gomez, A. N., Kaiser, L., and Polosukhin, I. Attention is all you need.(nips), 2017. *Advances in neural information processing systems*, 30, 2017.

Wiatrak, M., Albrecht, S. V., and Nystrom, A. Stabilizing generative adversarial networks: A survey. *ArXiv preprint*, abs/1910.00927, 2019. URL <https://arxiv.org/abs/1910.00927>.

Yu, J., Xu, Y., Koh, J. Y., Luong, T., Baid, G., Wang, Z., Vasudevan, V., Ku, A., Yang, Y., Ayan, B. K., et al. Scaling autoregressive models for content-rich text-to-image generation. *Transactions on Machine Learning Research*, 2(3):5, 2022.

Zhang, Z., Zhang, R., Li, Z., Bengio, Y., and Paull, L. Perceptual generative autoencoders. In *Proceedings of the 37th International Conference on Machine Learning, ICML 2020, 13-18 July 2020, Virtual Event*, volume 119 of *Proceedings of Machine Learning Research*, pp. 11298–11306. PMLR, 2020. URL <http://proceedings.mlr.press/v119/zhang20ab.html>.

Zheng, Z., Peng, X., Yang, T., Shen, C., Li, S., Liu, H., Zhou, Y., Li, T., and You, Y. Open-sora: Democratizing efficient video production for all, 2024. URL <https://github.com/hpcaitech/Open-Sora>.

Zhuang, J., Dvornik, N. C., Tatikonda, S., and Duncan, J. S. MALI: A memory efficient and reverse accurate integrator for neural odes. In *9th International Conference on Learning Representations, ICLR 2021, Virtual Event, Austria, May 3-7, 2021*. OpenReview.net, 2021. URL https://openreview.net/forum?id=blfSjHeFM_e.

A. Experimental details

Our models are implemented with PyTorch, and our experiments are conducted on A100 GPUs. We by default cast the model to *bfloat16*, which provides significant memory savings, with the exception of the likelihood task where we found that *float32* is necessary to avoid numerical issues. All of our jobs are finished within 14 days of training, though we believe that the models should get better if trained longer. We summarize the hyperparameters for our best jobs in Table 6.

Table 6. Hyper parameters for the best performing model on each task.

Task	Patch Size	Channels	Num Flows	Layers per Flow	Input Noise	Batch size	Epochs	Num GPUs
Uncond ImageNet 64x64 (likelihood)	2	768	8	8	$\mathcal{U}(0, \frac{1}{128})$	384	60	32
Uncond ImageNet 64x64 (generation)	2	768	8	8	$\mathcal{N}(0, 0.05^2)$	256	200	8
Cond ImageNet 64x64	2	768	8	8	$\mathcal{N}(0, 0.05^2)$	256	200	8
Cond ImageNet 128x128	4	1024	8	8	$\mathcal{N}(0, 0.15^2)$	768	320	32
Cond AFHQ 256x256	8	768	8	8	$\mathcal{N}(0, 0.07^2)$	256	4000	8

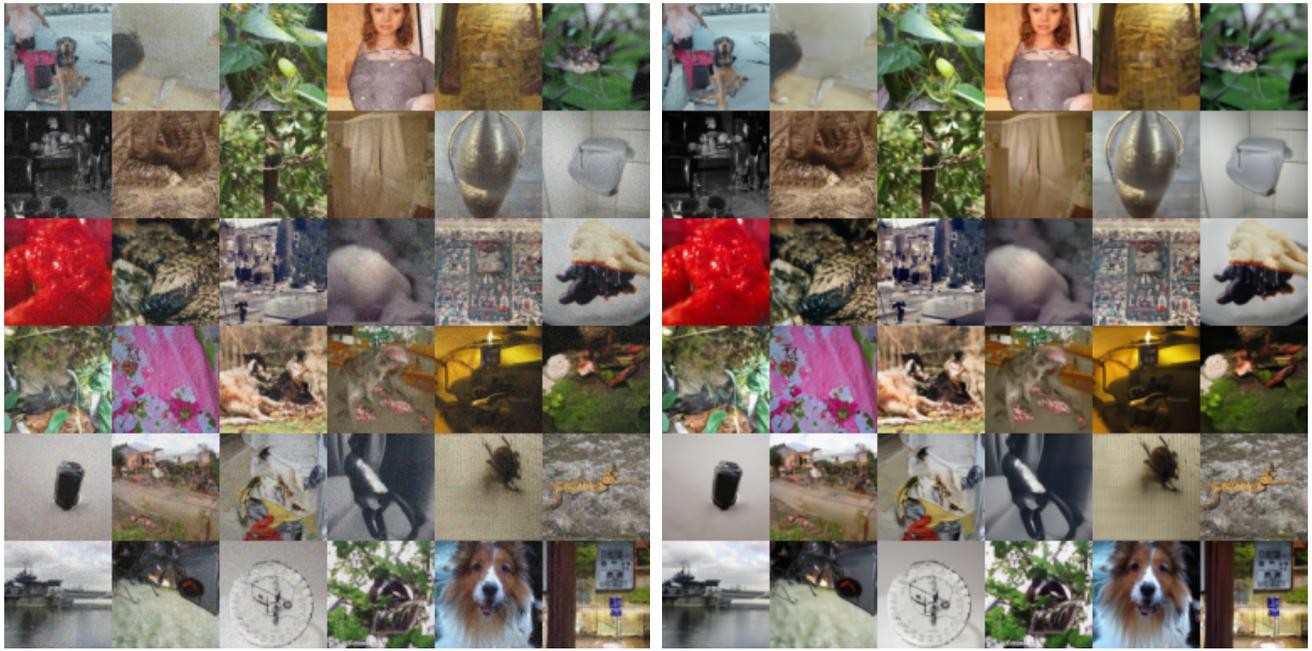
B. Inference Implementation

Although our main focus in this paper has been on training capable generative models, it is still worth commenting on the sampling efficiency of our method. Sampling from a TARFLOW involves reversing a series of causal Transformers. Unlike the training model where the autoregressive flow can be computed in parallel with causal masks, the reverse step is inevitably sequential with respect to the sequence direction. In practice, we resort to a KV-cache based implementation, which is a standard practice in the context of LLMs, and we found that it greatly speeds up the sampling over a naive implementation. For instance, sampling from a guided batch of 32 samples from the 2-768-8-8- $\mathcal{N}(0, 0.05^2)$ ImageNet 64x64 model takes about 2 minutes on a single A100 GPU. Although efficient sampling is not the focus of this work, we believe that there is great room for improvement in this regard, and we leave it as future work.

Another component in our sampling pipeline is the score based denoising step. The time of this step is equal to two forward model calls, which usually happens in a matter of seconds. A practical bottleneck is that this step is more memory consuming than the flow reverse step, due to the need of caching all intermediate activations for back propagation. In theory, this can be further alleviated by adopting techniques like gradient checkpointing, essentially trading time for memory.

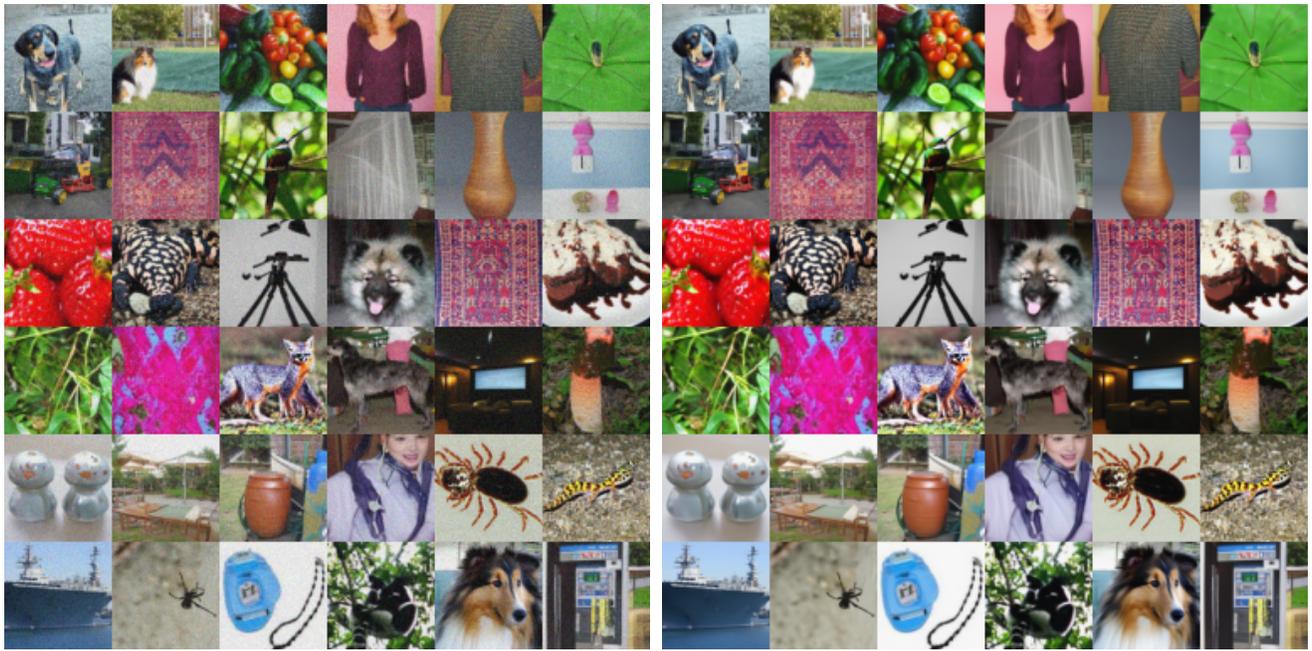
C. Additional samples

Next we show more uncurated samples from four generation tasks, demonstrating the raw samples, guided samples as well as denoised samples in Figure 9, 10, 11 and 12.



(a) guidance $w = 0$ (no guidance), noisy

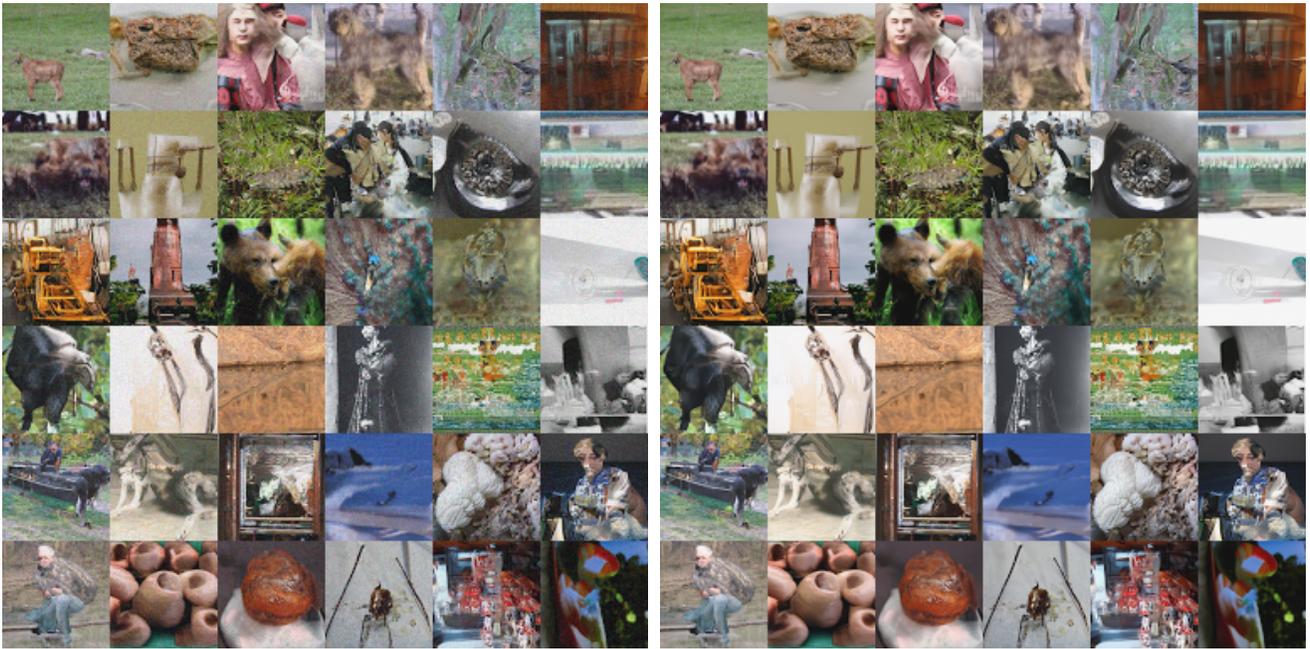
(b) guidance $w = 0$ (no guidance), denoised



(c) guidance $w = 2$, noisy

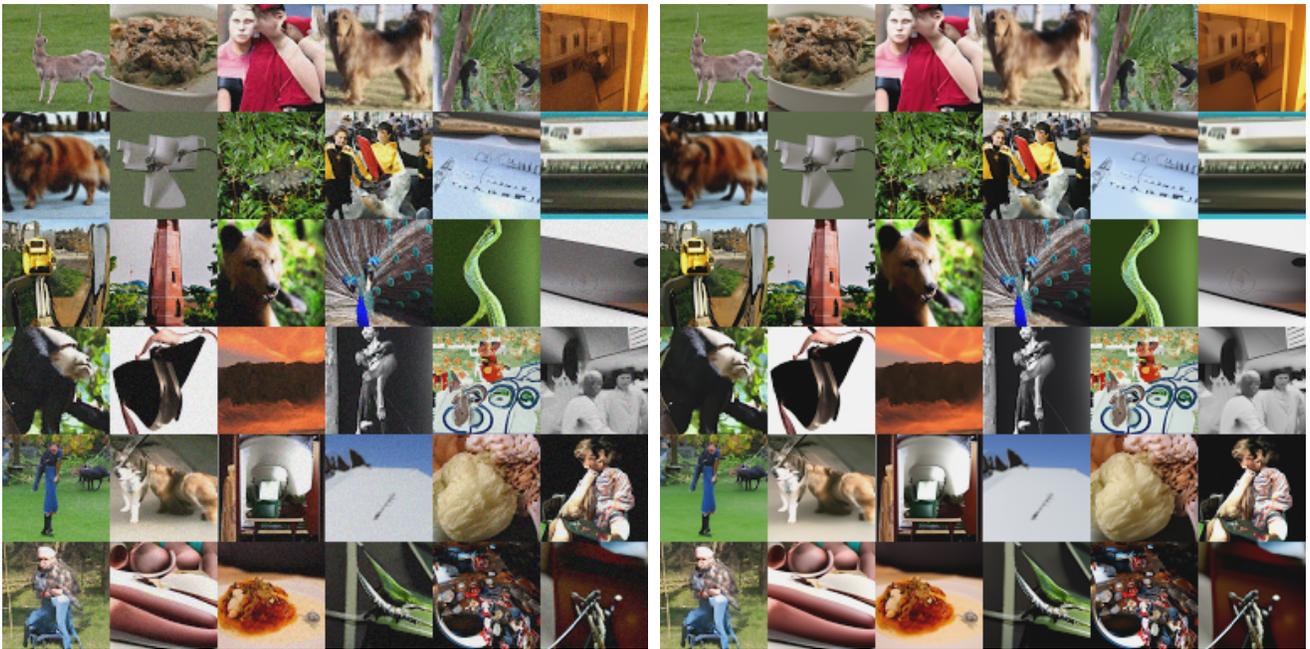
(d) guidance $w = 2$, denoised

Figure 9. Uncurated samples with a fixed set of initial noise from the model trained on conditional ImageNet 64x64.



(a) guidance $w = 0$ (no guidance), noisy

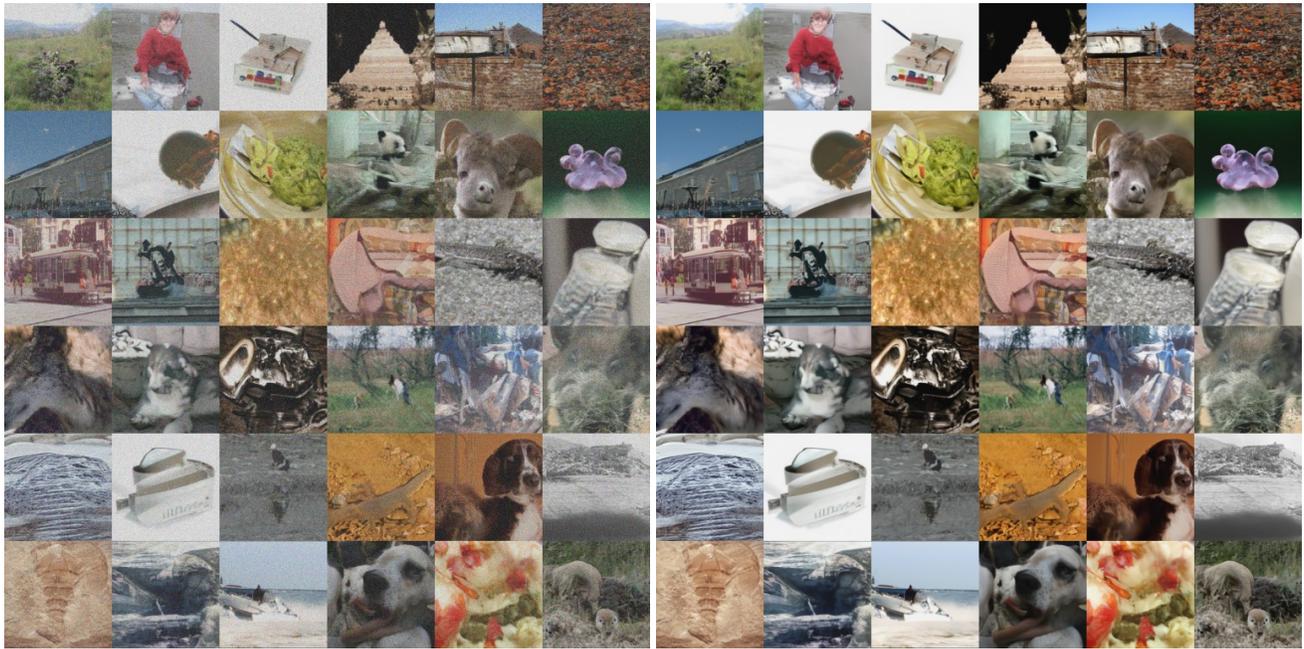
(b) guidance $w = 0$ (no guidance), denoised



(c) guidance $w = 0.15, \tau = 0.2$, noisy

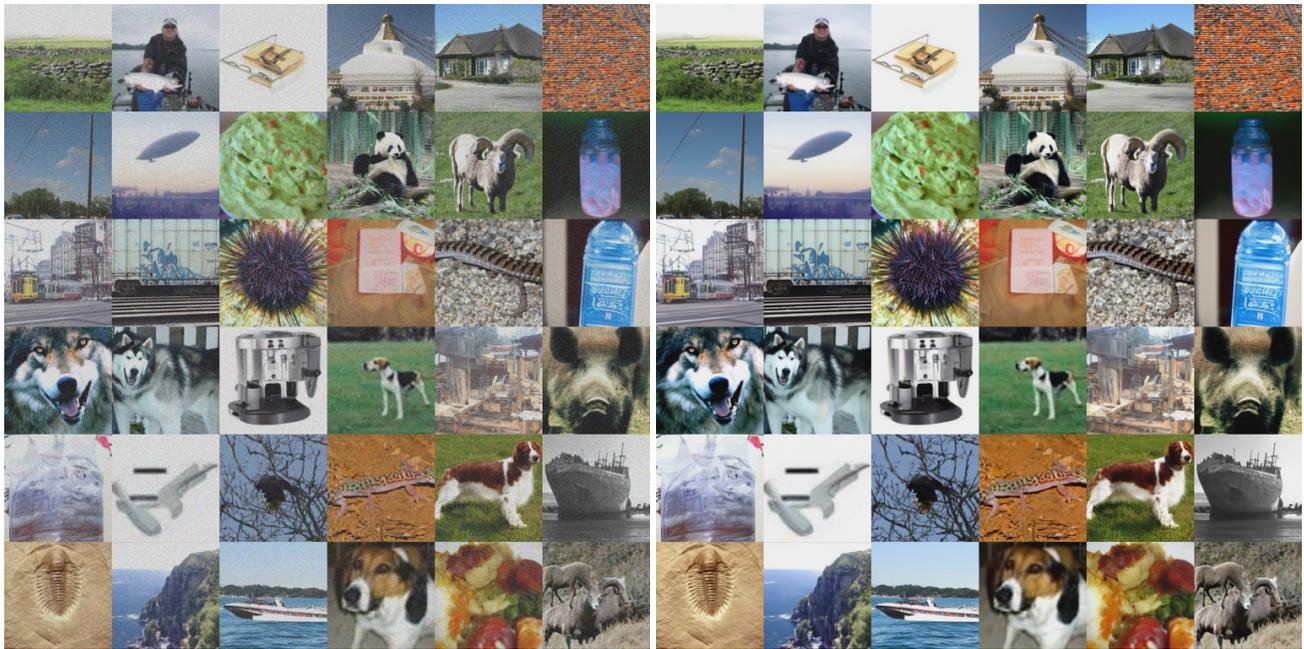
(d) guidance $w = 0.15, \tau = 0.2$, denoised

Figure 10. Uncurated samples with a fixed set of initial noise from the model trained on unconditional ImageNet 64x64.



(a) guidance $w = 0$ (no guidance), noisy

(b) guidance



(c) guidance $w = 2.5$, noisy

(d) guidance $w = 2.5$, denoised

Figure 11. Uncurated samples with a fixed set of initial noise from the model trained on conditional ImageNet 128x128.



(a) guidance $w = 0$ (no guidance), noisy

(b) guidance $w = 0$ (no guidance), denoised



(c) guidance $w = 2$, noisy

(d) guidance $w = 2$, denoised

Figure 12. Uncurated samples with a fixed set of initial noise from the model trained on conditional AFHQ 256x256.